The constitution of the welded joint in the GX4CrNi13-4 stainless steel

Boštjan Markoli in Savo Spaić

Oddelek za materiale in metalurgijo, Naravoslovnotehniška fakulteta, Ljubljana

Received: December 1, 2003 **Accepted:** December 10, 2003

Abstract: The constitution of the base material (GX4CrNi13-4) and the filler material (CN 13-4IG) was investigated in initial and heat-treated state using modern investigative techniques. The base material and the weld have the same constitution with martensite α_M as matrix, and α_{Fe}- and α_{Fe}-ferrite along with precipitates of $(Cr, Fe)_{23}C_6$ carbide. The hardness of the weld is lowered and more equal through the weldment after the stage III heat treatment. The weldment is free of typical welding defects such as porosity, macro- and microcracks, inclusions etc.

Key words: constitution, microstructure, welding, stainless steel

Introduction

Welding is a widely used joining technique also suitable for, e.g., to correct typical casting defects occurring in manufacturing turbines for water power plants. In order to produce durable defect free joints in GX4CrNi13-4 stainless steel turbines, which are also corrosion resistant the appropriate welding process as well as convenient filler material has to be chosen. Welding under CO_2 with DC and polarity (+), and CN 13-4 IG as filler material seem to meet these requirements [1-3]. The usage of CO_2 prevents the gas intake thus porosity and consequently crack formation in and around the weld [4, 5]. The chemical composition of the filler material insures the constitution and microstructure, which is very similar to the constitution and microstructure of the base material [6], the addition of ruthenium and rhodium [7-18] in filler material on the other side improves the corrosion resistance of the weldment.

Since the welding process is accompanied with fast crystallisation of the molten metal in the bead there is unavoidable presence of microsegregation of base and alloying elements as well as strain. This means that heat treatment of the weldment is needed to eliminate the initial morphology, microsegregation in the weld and anneal the matrix thus lowering the strain in the weld and surrounding base material. The heat treatment procedure has to be followed precisely to achieve the intended constitution and microstructure of the weldment.

In this paper the constitution and development of microstructure of the base material and the weld in as-welded and heat-treated state was investigated using metallograpic methods, such as: optical microscopy, scanning electron microscopy with energy-dispersive spectroscopy, X-ray phase analysis and hardness measurements (HV 0.5).

Scientific paper

EXPERIMENTAL

The GX4CrNi13-4 stainless steel was analysed in as cast and heat-treated state. The filler material (consumable) CN 13-4 IG was also analysed in as delivered commercial state and both as welded and heat-treated state. The weldment was cut into suitable sized specimens as shown in the Figure 1 [19], which were analysed using optical microscopy, REM with energy-dispersive spectroscopy, X-ray phase analysis and hardness measurements (HV 0.5). The chemical composition (Table 1) of base material GX4CrNi13-4 and filler material CN 13-4 IG was also checked with energy-dispersive spectroscopy.

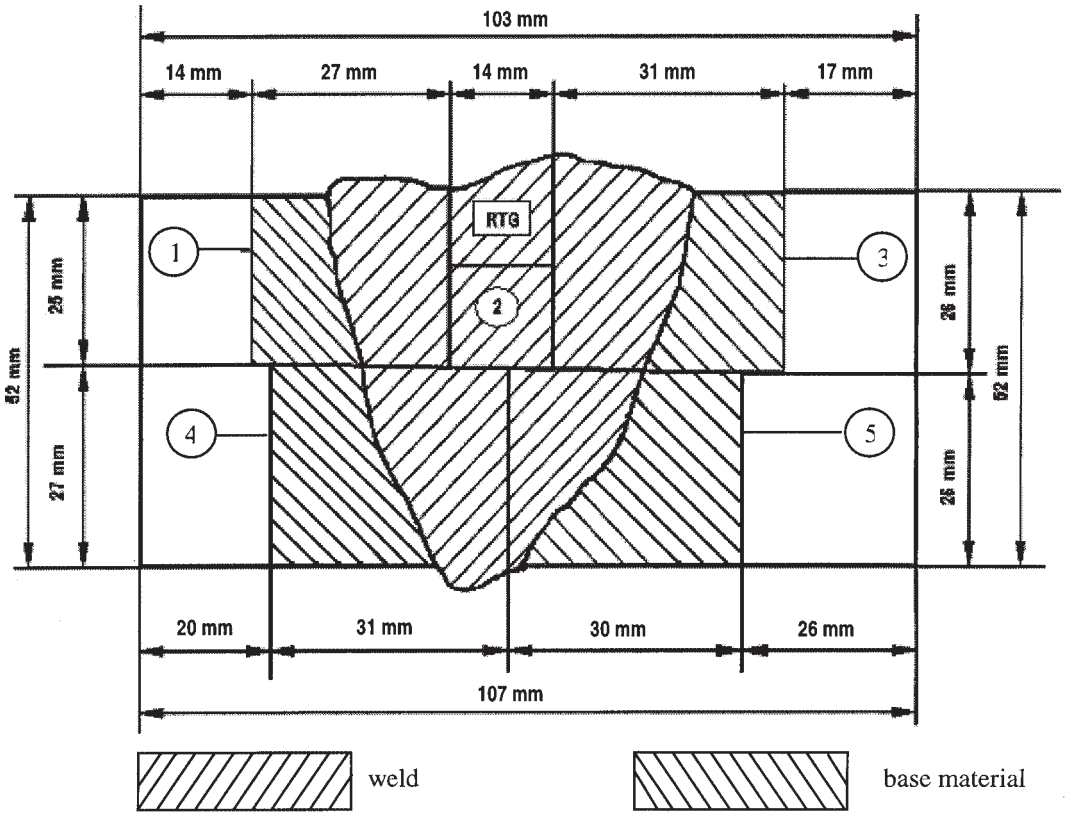

Figure 1. Schematic presentation of specimen assembling for investigation:
specimens denoted with numbers 1-5, specimen No. 2 was also used for X-ray analysis.

Table 1. Chemical composition of the base material (GXCrNi13-4) and filler material (CN 13-4 IG) in mass %

Element	Base material	Filler material
C	0.02	0.035
Si	0.43	0.30
Mn	0.68	-
P	0.033	-
S	0.010	-
Cr	12.9	12.20
Mo	0.56	0.50
Ni	3.72	4.50
Ru	-	0.754
Rh	-	0.265

The base material GXCrNi13-4 was heat treated prior to welding as follows:
Stage I: heating (65 °C/h) to 1050 °C and holding for 6^h, then cooling in the air.
Stage II: annealing (40 °C/h) to 610 °C and holding for 6^h, then cooling in the furnace (40 °C/h) to 250 °C, then cooling in the air.
Stage III: annealing (40 °C/h) to 590 °C and holding for 6^h, then cooling in the furnace (40 °C /h) to 250 °C, then cooling in the air.
The weldment itself was also heat treated in the same way as the base material in the stage III.

Results and discussion

The optical micrograph (Figure 2) of the base material in the heat-treated state show the presence of martensite matrix α_M with typical lath-like morphology which is in accordance with reference [2]. Within the microstructure of the base material there is also evidence of light phase in form of small islets, which are clearly seen in the Figure 3. The EDS analyser mounted on the REM revealed the composition of the light phase (Table 2), which excludes the presence of the σ-CrFe phase.

This has further been confirmed by the X-ray phase analysis of the base material in the heat-treated state (Figure 4). The diffraction pattern in the Figure 4 shows presence of the multicomponent martensite matrix α_M, multicomponent δ_{Fe}-ferrite, $(Cr, Fe)_{23}C_6$ type carbide, and multicomponent α_{Fe}-ferrite. Closer inspection of the diffraction pattern namely reveals the split of peaks for the major {110}, {200}, {211} and {220} planes of martensite α_M and that intensity for the δ_{Fe}-ferrite are very low. According to the chemical composition of base material in the Schäffler diagram [1] the microstructure should consist

Table 2. EDS analysis of the light phase (islets)

Element	Si	Cr	Mn	Fe	Ni	Mo
Mass %	1.166	19.220	0.247	77.506	1.106	0.756

Figure 2. Microstructure of the base material (GX4CrNi13-4) in the heat-treated state

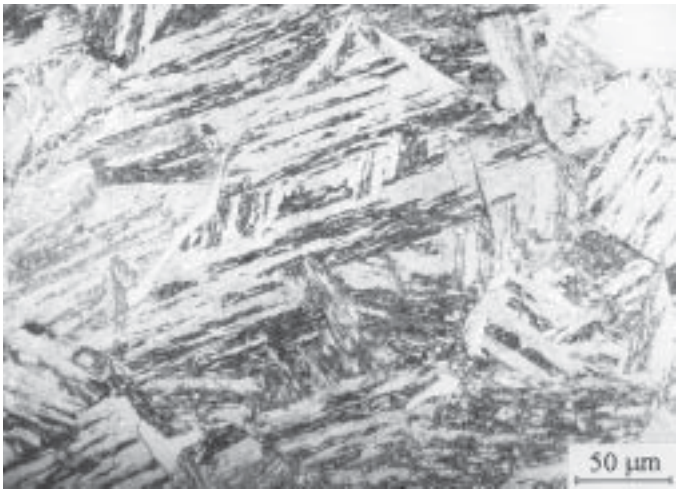

Figure 3. Microstructure of the base material (GX4CrNi13-4) in the heat-treated state: presence of the white islets of multicomponent d_{Fe}-ferrite phase

of martensite α_M and approximately of 15 % ferrite. There is no clear distinction or explanation in the reference [1] whatsoever, if this ferrite is either δ_{Fe}- or α_{Fe}-ferrite. Thus it can be concluded based on the assessment of the volume fraction of the microstructural constituents by optical microscopy (Figure 3), X-ray phase analysis and comparison of reference data [1] and the constitution of the Fe-rich corner of the binary Fe-Cr system [6] that the multicomponent α_{Fe}-ferrite is present in the microstructure of the base material.

Since the chemical composition of the base material and filler material are very similar (Table 1) the same constitution can be expected in the weld itself. There is on the other hand compositional difference with regard

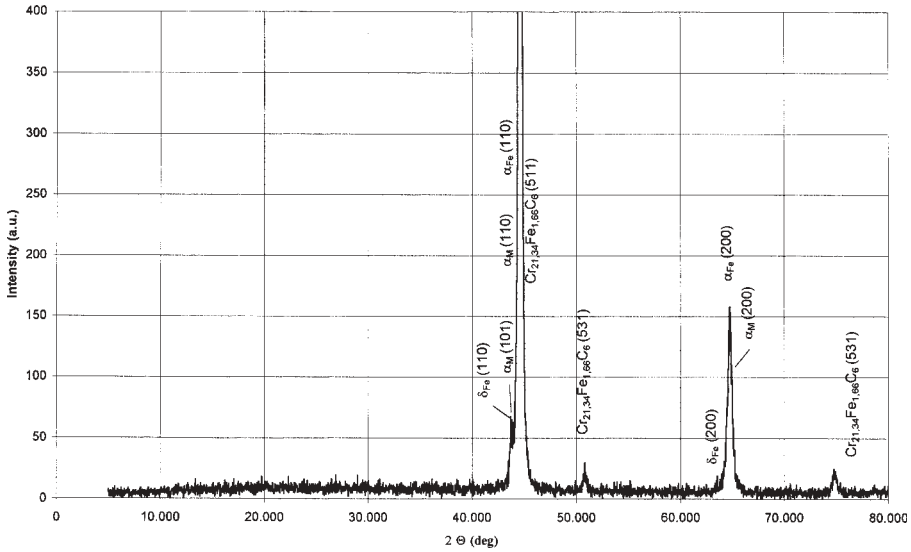

Figure 4. X-ray analysis of the base material (GX4CrNi13-4) in the heat-treated state

to presence of ruthenium and rhodium in filler material. These two elements are added with improvement of corrosion resistance of the weldment in mind as described in relevant references [7-18].

Macroscopic investigations of the weldment in as-welded state

The macrostructure of the weld itself as well as of the surrounding base material was revealed using ADLER as etchant (etching time up to 40 sec) along with the hardness measurements (HV 0.5) across the weldment.

From the Figure 5 of the weldment in the as welded state the formation of distinct zones within the heat-affected zone (HAZ) can be seen. The hardness measurements (HV 0.5) show that the average base material hardness is of ~260 HV, which increases through the darker zone on the left to ~340 HV, and reaches maximum in the light zone next to fusion line with ~385 HV. The hardness decreases through the weldment toward the right side of the weld and reaches ~360 HV in the light zone. This is followed by a sharp drop through the dark zone to ~260 HV, which is the hardness of the base material. The difference in the hardness between left and right side of the weldment is caused by the welding procedure. The welding started at the right side and continued towards the left side until the gap was filled. This means that the martensite α_M in the first bead on the right side is more annealed than the martensite α_M in all subsequent beads, especially in the last bead on the left side. The annealing is more pronounced on the right side of the weldment because the fusion heat of each bead made during the welding process is also transferred through the beads made at the beginning of the welding, that is the right side. The difference in the hardness on the left and right side of the weldment is eliminated during the heat treatment.

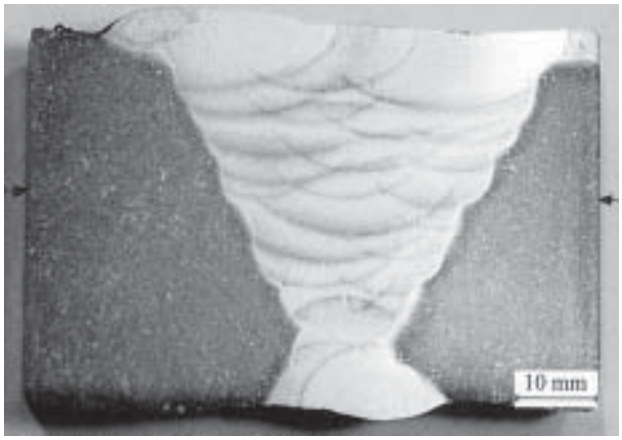

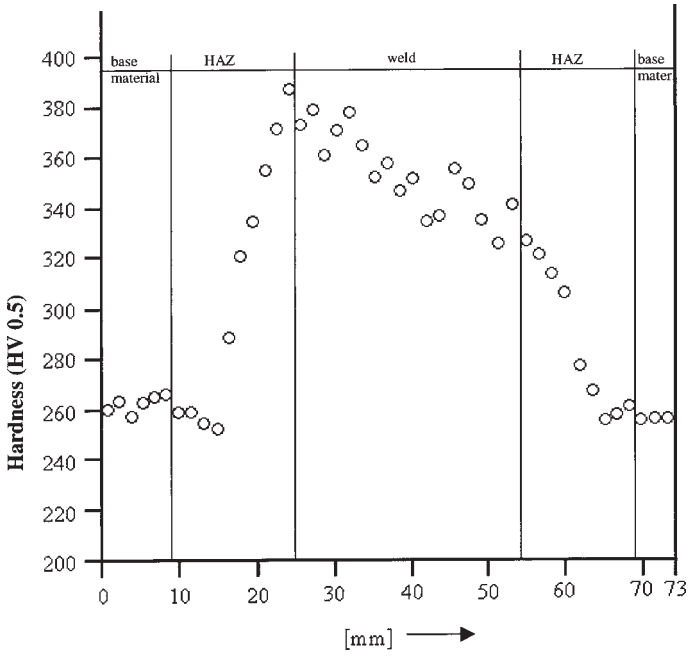

Figure 5. Macrostructure and hardness (HV 0.5) across the weldment in as-welded state

MACROSCOPIC INVESTIGATIONS OF THE WELDMENT IN THE HEAT-TREATED STATE

The Figure 6. reveals the development of the macrostructure in the weldment after the stage III heat treatment. The HAZ is more distinct from the base material with pronounced darker zone and thinner lighter zone next to the fusion line. Macrostructure of each bead (totally 26 beads made) with typical columnar morphology can also be recognized.

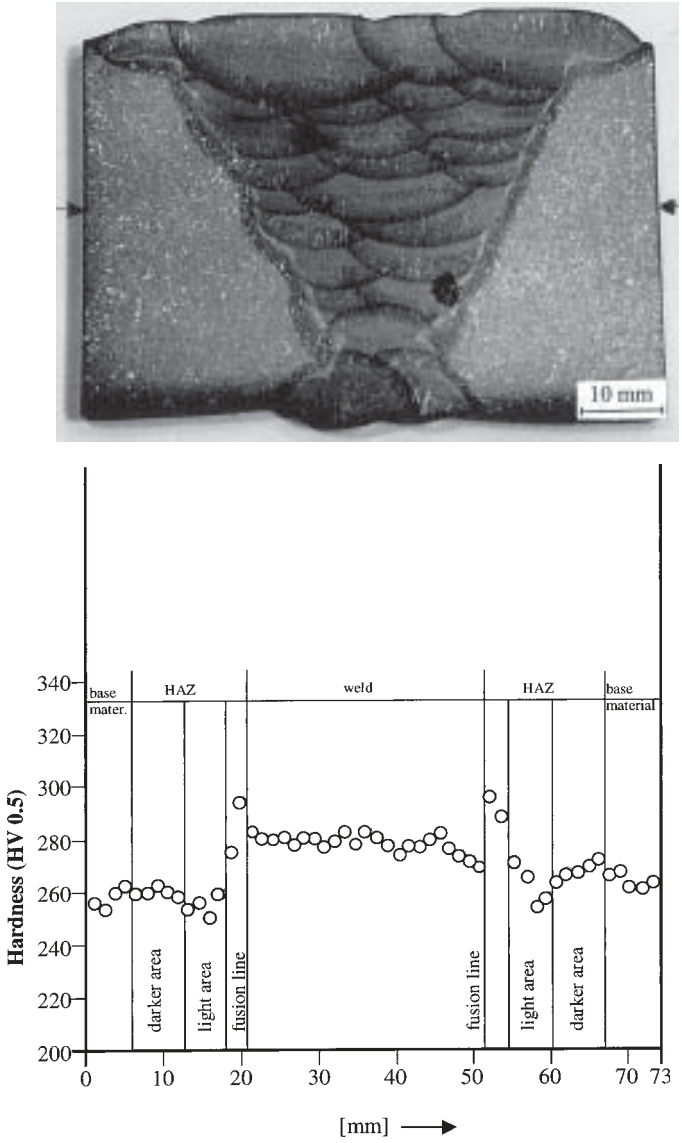

Figure 6. Macrostructure and hardness (HV 0.5) across the weldment in heat-treated state

Hardness measurements across the weldment show that the overall hardness is lower and more equalized than in the as-welded state. Still the hardness of the weld itself is higher with ~280 HV from the hardness of the base material with ~260 HV. The hardness is also highest in the light zone next to the fusion line. This is on the other hand the area, which is most likely to initiate or to form microcracks [4] when material is exposed to cyclic mechanical strain.

Comparison of macrostructure in Figures 5 and 6 shows that the weld and the HAZ as well as the base material in as-welded and heat-treated state are actually completely free

of typical welding defects apart from one localized inclusion in the weld after heat treatment (Figure 6).

MICROSCOPIC INVESTIGATIONS OF THE WELDMENT

In the micrograph of the weld prior to the stage III heat treatment (Figure 7) made by optical microscopy the columnar-dendritic morphology is evident which is typical for higher crystallisation rates that can be expected during the process of welding. This is also associated with occurrence of microsegregation of base and alloying elements and enrichment of the base material next to the fusion line mostly with the nickel as confirmed by the EDS analysis of the area adjacent to the fusion line (Figure 8 and Table

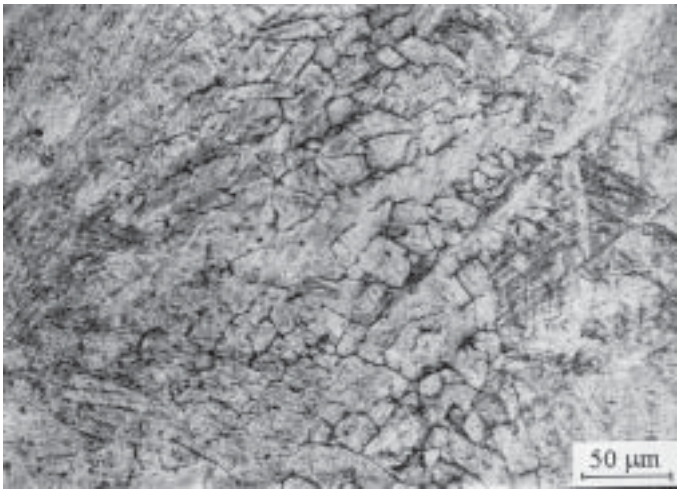

Figure 7. Microstructure of the weld (filler material) prior to heat treatment

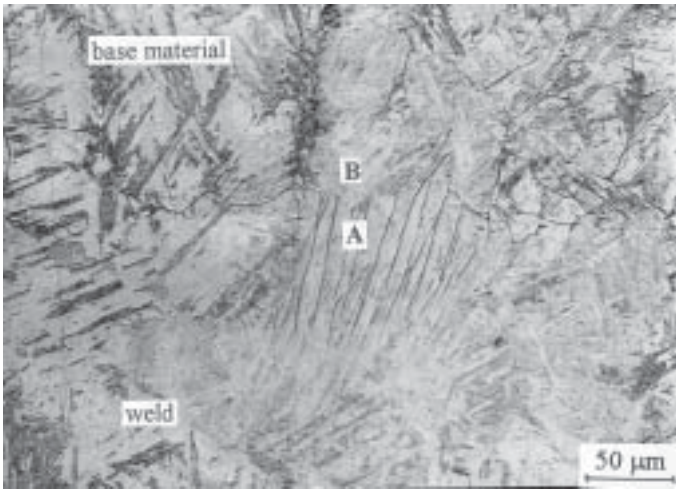

Figure 8. Optical microscopy of the fusion line in the weldment in as-welded state: A-weld; B-base material in conjunction with Table 3

Table 3. EDS analysis of the area adjacent to the fusion line in conjunction with Figure 8

Filler material (weld) A		Base material B	
Element	Mass %	Element	Mass %
Al	0.039	Al	0.004
Si	0.558	Si	0.254
Cr	11.015	Cr	11.772
Mn	0.353	Mn	0.368
Fe	83.225	Fe	83.750
Ni	4.626	Ni	3.702
Ru	0.152	Ru	0.039
Rh	0.033	Rh	0.112

3). The EDS analysis in addition revealed the diffusion of ruthenium and rhodium from the filler material in the weld into the base material (Table 3), with both elements added to increase the corrosion resistance of the weldment as described in reference [7-18].

The initial morphology of the weld is eliminated during the heat treatment (Figure 9) where some remains of this morphology are mostly restricted to the root and surface of the weld. The microstructure of the weld has finer martensitic laths than in the base material and the fusion line seen in the Figure 8 becomes wider and actually disappears as such during the heat treatment. The constitution of the weld and base material are actually the same as established with the X-ray analysis of the weld in heat-treated state (Figure 10) and comparison of both diffraction patterns (Figure 4 and Figure 10). The matrix of the weld is lath-like martensite α_M (Figure 9) next to δ_{Fe}-ferrite which appears in the microstructure as white spots or islets,

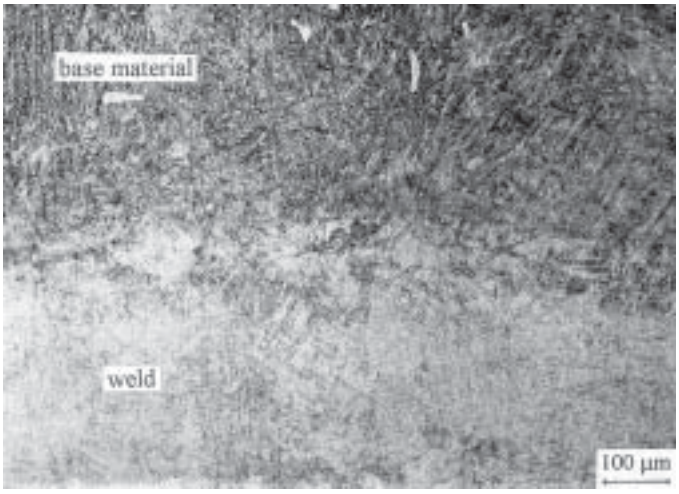

Figure 9. Microstructure of the weld in heat-treated state

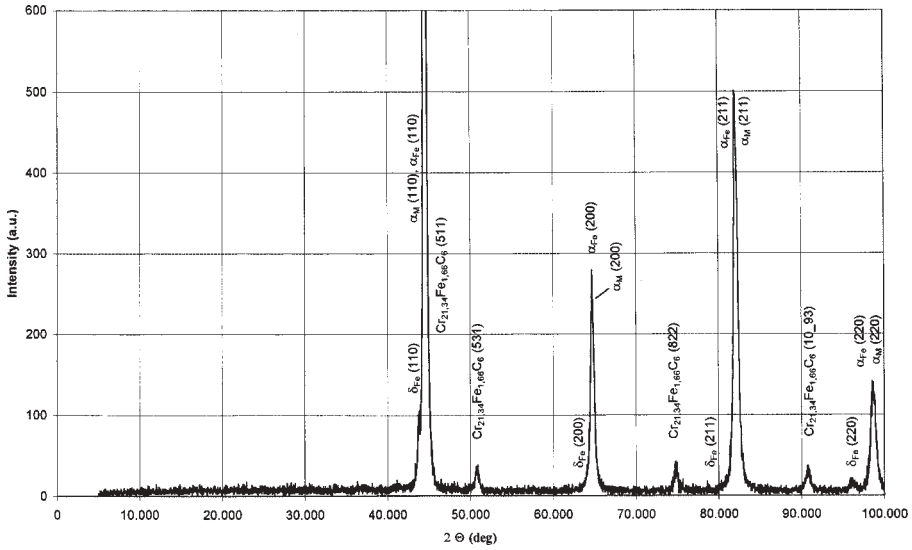

Figure 10. X-ray analysis of the weld in the heat-treated state

$(Cr, Fe)_{23}C_6$ carbide and α_{Fe}-ferrite which is very likely incorporated in the matrix α_M which also the case for the base material in the heat-treated state (Figure 4). The $(Cr, Fe)_{23}C_6$ carbide precipitates are very small and are apparently below the detection limit of the optical microscope.

CONCLUSIONS

From the results of the macro- and microscopic investigations of the weld (CN 13-4 IG) and base material GX4CrNi13-4 it is clear that the constitution of both are actually the same with martensite α_M as matrix and both α_{Fe}- and δ_{Fe}-ferrite along with $(Cr, Fe)_{23}C_6$ carbide as small precipitates. The initial morphology of the weld a well as the fusion line are eliminated during the heat treatment and the martensite matrix is annealed which results in lowering the hardness of the weld. The diffusion of the ruthenium and rhodium from the filler material in the weld into the base material was established which improves the corrosion resistance of the weldment. The weld and adjacent base material are free from typical welding defects apart from one localized inclusion.

References

[1] Lohrmann, R. (1984): MAGM-Schweißen hochlegierter Stähle. *DVS Berichte*, Schutzgas-Schweißen, Band 87, 54-60.

[2] *Alloying: Austenitic Stainless Steels With Emphasis on Strength at Low Temperatures*, ASM International, Metals Park Ohio 1988, pp. 225- 256.

[3] Düren, C., Müsch, H., Brühl, F. (1970): Schweissplattieren von Rohrleitungen im Kernreaktorbau, *DVS Berichte*, No. 15, 1970, pp. 47-58.

[4] Bouchard, P. J., Withers, P. J., McDonald, S. A. Heenan, R. K. (2004): Quantification of creep cavitation damage around crack in a stainless steel pressure vessel. *Acta Materialia*, Vol. 52, pp. 23-43.

[5] Lachmann, C., Nitschke-Pagel, Th., Wohlfahrt, H. (2003): Bedeutung von Eigenspannungsabbau und mikrostrukturellen Veränderungen für die Lebensdauervorhersage schwingbeanspructher Scweißverbindungen. *Z. Metallkde.*, Vol. 94, pp. 640-648.

[6] Massalski, T. B., Okamoto, H., Subramanian, P. R., Kasprzak, L. (eds.) (1990): *Binary Alloys Phase Diagrams*, 2nd ed, ASM, Metals Park, Ohio.

[7] Myburg, G., Varga, K., Barnard, W. O., Baradlai, P., Tomcsányi, Potgieter, J. H., Louw, C. W., Van Staden, M. J. (1998): Surface composition of Ru containing duplex stainless steel after passivation in non-oxidizing media. *Applied Surface Science*, Vol. 136, pp. 29-35.

[8] Potgieter, J. H. (1996): The effect of ruthenium on the corrosion behaviour of a 22 mass % chromium ferritic stainless steel in 1 M sulphuric acid. *Journal of Materials Science Letters*, Vol. 15, pp. 1408-1411.

[9] Wolff, I. M., Iorio, L. E., Rumpf, T., Scheers, P. V. T., Potgieter, J. H. (1998): Oxidation and corrosion behaviour of Fe-Cr and Fe-Cr-Al alloys with minor alloying additions. *Materials Science and Engineering*, Vol. 241, pp. 264-276.

[10] Potgieter, J. H., Ellis, P., van Bennekom, A. (1995): Investigation of the Active Dissolution Behaviour of a 22% Chromium Duplex Stainless Steel with Small Ruthenium Additions in Sulphuric Acid. *ISIJ International,* Vol. 35, No. 2, pp. 197-202.

[11] Tjong, S. C., Lin, W. B., Ku, J. S., Ho, N. J. (1996): Fe-Cr-Ni-Mo-Ru Alloys Produced by Laser Surface Alloying. *Surface engineering*, Vol.12, No. 3, pp. 246-250.

[12] Potgieter, J. H., van Benekom, A. (1995): The effect of varying ruthenium content on the corrosion behaviour of two cathodically modified superferritic stainless steel. *Canadian Metallurgical Quarterly*, Vol. 34, No. 2, pp. 143-146.

[13] van Staden, M. J., Roux, J. P. (1990): The controlled oxidation of the high chromium steel alloys Fe40Cr and Fe40Cr3Ru. *Applied Surface Science*, Vol. 44, pp. 263-269.

[14] Cowan, R. L., Hettiarachchi, Law, R. J., Miller, W. D., Diaz, T. P. (2001): Experience with Noble Chemical Addition in BWRs. *VGB PowerTech*, Vol. 4, pp. 81-86.

[15] Hasström, M., Jäglid, U., Petterson, J. B. C. (2000): Desorption kinetics at atmospheric pressure: alkali interactions with rhodium and steel surface. *Applied Surface Science*, Vol. 161, pp. 291-299.

[16] Tjong, S. C. (1990): Self-passivation of Fe-Cr.PGM alloys in reducing acid studied by electrochemical and electron spectroscopic techniques. *Applied Surface Science*, Vol. 45, pp. 301-318.

[17] Baradlai, P, Potgieter, J. H., Barnard, W. O., Tomcsány, L., Varga, K. (1995): Investigations of spontaneous passivation of stainless steels modified with ruthenium. *Materials Science Forum*, Vol. 185-188, pp. 759-768.

[18] Takeda, S., Nagai, T., Takeuchi, M. (1996): Corrosion performance of stainless steel in nitric acid solutions containing fission products. *Zairyo-to-Kankyo*, Vol. 45, pp. 277-283.

[19] Vrban, R.: Diplomsko delo, Visokostrokovni študij, Naravoslovnotehniška fakulteta, Univerza v Ljubljani.

Konstitucija zvarjenega spoja nerjavnega jekla GX4CrNi13-4

Povzetek: Z raziskavalnimi metodami s področja fizikalne metalurgije je raziskana konstitucija osnovnega (GX4CrNi13-4) in dodajnega materiala (CN 13-4 IG) v izhodnem in toplotno obdelanem stanju. Ugotovljeno je, da je matrica osnovnega in dodajnega materiala martenzit α_M, poleg α_{Fe}- in δ_{Fe}-ferita ter izločkov zmesnega karbida $(Cr, Fe)_{23}C_6$.

V mikrostrukturi zvara pred toplotno obdelavo je razvidno izoblikovanje značilnih področij toplotno vplivane cone z izrazito stebričasto morfologijo ob talilni črti ter svetlimi otočki δ_{Fe}-ferita. Toplotno vplivana cona se v zgornjem delu "V" zvara razpenja čez širše področje osnovnega materiala kot v bližini korena zvara. Po toplotni obdelavi talilna črta praktično izgine mestoma pa se ohranijo mikrostrukturne značilnosti izhodnega stanja zvara.

Meritve trdote HV 0.5 so pokazale enakomernejši potek le-te skozi zvar po toplotni obdelavi, pri čemer se ohrani značilni maksimum trdote ob sicer zabrisani talilni črti, ki pa je manj izrazit glede na maksimum trdote pred toplotno obdelavo.

Iz makroskopskega pregleda zvara sledi, da je zvar brez značilnih napak varjenja kot so poroznost, makro-in mikrorazpoke itd., razen enega lokaliziranega vključka, kar kaže na primerno izbran postopek in režim varjenja kot tudi dodajni material.